Proceedings of ISFOG 2025
5TH INTERNATIONAL SYMPOSIUM ON
FRONTIERS IN OFFSHORE GEOTECHNICS
Nantes, France | June 9-13 2025

ISBN 978-2-85782-758-0

Impact of local scour on the development of the failure envelope for suction caisson foundations

Zhuang JIN*
Shenzhen University, Shenzhen, China

Yin-Fu JIN
Shenzhen University, Shenzhen, China

Meng-Huan GUO
Shenzhen University, Shenzhen, China Meng-Huan GUO
Shenzhen University, Shenzhen, China

**jinzhuang@szu.edu.cn (corresponding author)*

ABSTRACT: Local scouring significantly undermines the load-bearing capacity of suction caisson foundations and poses a daunting challenge to the integrity of offshore structures. This study numerically addresses the impact that the size and shape of the local scour hole have on both the monotonic bearing capacities and failure envelopes of suction caisson embedded in sandy soil. Different loading conditions - individually and combined - by integrating local scour parameters such as scour depth (S_d), scour width (S_w) and scour angle (φ) while maintaining realistic scour proportions are carefully evaluated. The obtained results show that (1) scour depth has a stronger influence on the ultimate bearing capacity than the influences of scour width and angle; (2) the horizontal bearing capacity shows increased sensitivity to variations in scour depth; and (3) both the horizontal bearing capacity and the moment bearing capacity reach a plateau and a steady state manifest itself when the relative scour depth exceeds a threshold value of 0.9. An empirical formulation to characterize the failure envelope within the horizontal force-moment (*H-M*) plane is finally proposed, which properly considers the effect of scour depth. These findings provide a valuable reference for ensuring structural resilience to local scour phenomena.

Keywords: Local scour; failure envelope; caisson; bearing capacity; sand

1 INTRODUCTION

Suction caisson foundations are widely used in offshore engineering due to their ease of installation, high load capacity, and reusability (Houlsby and Byrne, 2004; Villalobos et al., 2009). However, local scour erosion around the foundation—can significantly impact their performance (Lin and Lin, 2019, 2020). Scour can be classified into general (erosion across the seabed) and local (erosion near foundations), with local scour often causing deeper erosion and more substantial reductions in bearing capacity (AASHTO, 2010). Influencing factors include water flow characteristics, caisson geometry, embedment depth, and soil properties (Arneson, 2013). A common approach to model local scour is by removing the top soil layer down to the estimated scour depth, typically representing the scour hole as an inverted truncated cone with parameters for scour depth (S_d), width (S_w), and angle (φ) (Liang et al., 2017; Lin et al., 2014).

Recent studies highlight the importance of considering local scour dimensions in foundation design, as these significantly impact bearing capacity, especially for lateral stability and load resistance (Chen et al., 2019; Liu et al., 2019). While monopiles in scoured environments have been well-studied, there is limited research on caissons under similar conditions. Existing studies generally consider single loading scenarios, although suction caisson foundations are exposed to combined environmental loads, such as waves, wind, and currents. Limited studies address the failure envelopes of suction caissons under local scour, though recent work by Guo et al. (2022) uses Finite Element Method (FEM) to evaluate how scour dimensions affect bearing capacity and failure limits, primarily in undrained soils.

This study seeks to fill gaps in understanding by examining failure envelopes for suction caissons in sandy soils under local scour. Using a validated 3D FEM model, the impact of scour depth, width, and angle on failure envelopes is assessed through extensive parametric cases. Additionally, a modified analytical formula is proposed to incorporate the effects of local scour on the failure envelope, offering a more realistic approach for caisson foundation design.

2 NUMERICAL MODEL

2.1 Numerical model setup

This study utilizes the commercial finite element software ABAQUS for analysis. The Mohr–Coulomb model is applied to capture the behavior of sandy soil. As shown in Figure 1, the numerical model spans a length of 20*D* and a depth of 4*L* (where *D* represents the diameter and *L* the length of the suction caisson), providing sufficiently large dimensions to mitigate boundary effects. A mesh convergence analysis is conducted to ensure both accuracy and computational efficiency, with the minimum mesh size set to *D*/50. The lateral boundaries are fixed in the horizontal direction, and all translational degrees of freedom are constrained at the model's base.

The suction caisson is modeled as a rigid body. For both the caisson and soil, 8-node linear brick elements with reduced integration (C3D8R) are used. The soil-foundation interface is represented with Coulomb contact, which includes both normal and tangential interaction responses (ABAQUS, 2014). Soil parameters were calibrated using an optimization-based identification method (Jin et al., 2017), grounded on test results from Houlsby et al. (2005). These parameters include a Young's modulus E of 36 MPa, Poisson's ratio ν of 0.3, friction angle ϕ of 36°, and cohesion c of 0 kPa. Additionally, the soil density is 1700 kg/m³, and the friction coefficient at the soil-caisson interface is 0.34 (k=tan(ϕ/2)).

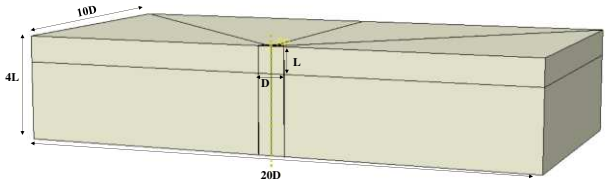

Figure 1 Numerical model setup for caisson foundation

2.2 Experimental setup

A small-scale field test by Houlsby et al. (2005) was simulated to validate the accuracy of the numerical model. This test featured a steel caisson with a diameter and skirt length of 2 m, with a 12 mm thick steel skirt plate. The caisson was subjected to a vertical load of 37.3 kN and a load eccentricity h of 17.4 m. Dense Baskarp sand with a unit weight of 19.5 kN/m³ was used as the test medium (Ibsen et al., 2005). The test procedure included phases of installation, loading, and disassembly. A wind turbine tower was mounted on the caisson to apply the loading, and horizontal load was applied by pulling the tower with a wire. Control of combined loading (horizontal force H and moment M) was achieved by adjusting the height of the tower.

2.3 Model calibration for caisson foundation

To demonstrate the robustness of the numerical model, a moment-rotation test was conducted on a caisson with dimensions of 2 m in both depth and width, following the procedure outlined by Houlsby et al. (2005). The test employed a slow displacement rate of 10 mm/s and a rotation rate of 0.5 degrees/s to minimize dynamic effects. As shown in Figure 2, the numerical results align closely with the experimental data, with the model effectively capturing the evolution of both moment and bearing capacity.

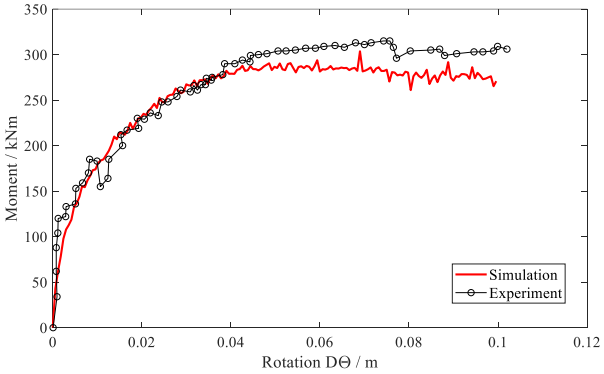

Figure 2 Comparison between simulation results and field measurements: moment M and rotation Dθ curve

3 INVESTIGATION OF BEARING CAPACITY CONSIDERING LOCAL SCOUR

A series of parametric investigations were conducted to analyze the influence of scour depth (S_d), scour angle (φ), and scour width (S_w) on the monotonic bearing capacity of the caisson. A schematic of the local scour setup is shown in Figure 3. In this phase of the study, force was applied using a displacement control method, with the specific geometries and loading angles illustrated in Figure 4. The ultimate pull-out capacity of the suction anchor was evaluated using two criteria: (1) the load at which the load-displacement curve begins to linearize is defined as the bearing capacity; and (2) if the displacement exceeds 0.1*D*, the load corresponding to 0.1*D* is taken as the bearing capacity (Jin Z. et al., 2019).

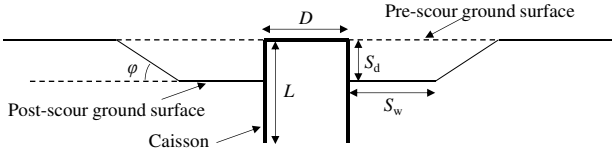

Figure 3 Diagram of local scour hole

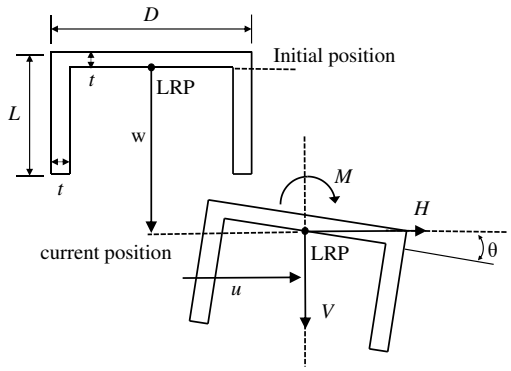

Figure 4 Loading and displacement conventions for a caisson foundation

3.1 Influence of scour depth

To investigate the influence of scour depth on the bearing capacity of caisson foundation, seven relative scour depths (S_d/L=0, 0.1, 0.3, 0.5, 0.7, 0.9, 1.0) are adopted for the simulations. A constant relative scour width S_w/D=0.5 and scour angle φ=30° are utilized.

The load-displacement curves for the caisson under horizontal and moment loading at various scour depths are shown in Figures 5 and 6, normalized as $H/\gamma D^3$ and $M/\gamma D^4$, respectively. The bearing capacity factors N_H for horizontal loading and N_M for moment loading are summarized in Figure 7. As scour depth increases, both horizontal and moment bearing capacities decrease noticeably. The reduction in horizontal bearing capacity follows a mostly linear trend with increasing scour depth, while moment capacity shows an inflection point at a relative scour depth of S_d/L=0.5. Horizontal capacity is more sensitive to scour depth, with an 80% reduction at S_d/L=1.0, compared to a 50% reduction for moment capacity.

Notably, as shown in Figure 7, when the relative scour depth exceeds 0.9, both horizontal and moment bearing capacities stabilize, indicating that further increases in scour depth no longer affect their capacities.

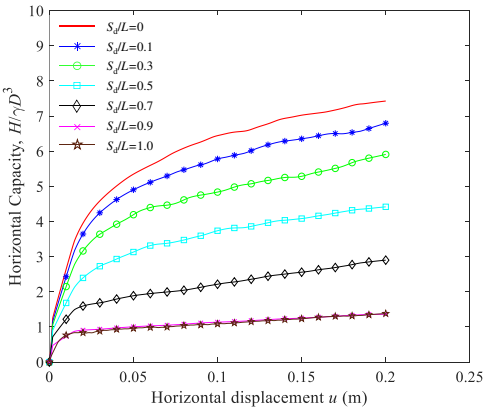

Figure 5 Horizontal loading-displacement curves of caisson with various depths

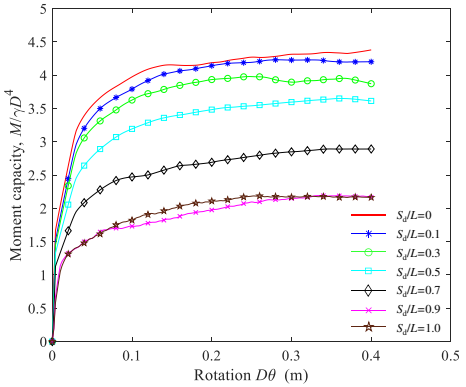

Figure 6 Moment loading-displacement curves of caisson with various depths

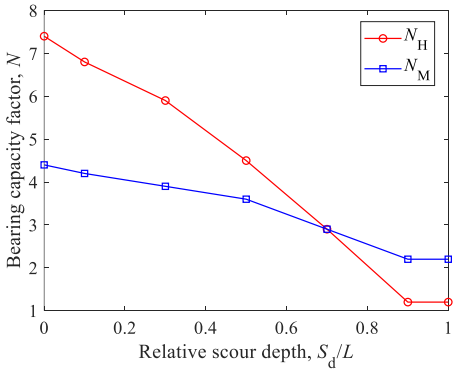

Figure 7 Bearing capacity factors with different relative scour depths

3.2 Influence of scour width

A comprehensive analysis was conducted on the caisson's response to six relative scour widths (S_w/D=0.5, 0.6, 0.7, 0.8, 0.9, 1.0), with a constant scour depth (S_d/L=0.3) and scour angle (φ=30°) set as a baseline. Figure 8 provides a detailed illustration of the effects of scour width on the normalized bearing capacity of the caisson.

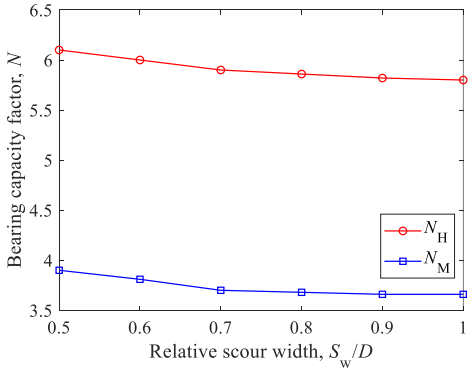

Figure 8 Bearing capacity factors with different relative scour width

Trend analysis shows that both horizontal and moment bearing capacities decrease gradually as scour width increases, with a slowing rate of decay. This suggests that as scour width continues to grow, bearing capacity may eventually stabilize, similar to the

pattern observed with scour depth. These findings underscore the importance of considering multiple scour parameters to achieve accurate predictions and robust designs for caisson foundations in sandy soil.

3.3 Influence of scour angle

This section explores the impact of scour angle on caisson bearing capacity, examining six angles (φ=15°, 22.5°, 30°, 37.5°, 45° and 60°). A fixed scour depth (S_d/L=0.3) and width (S_w/D=0.5) are used to standardize comparisons. Figure 9 illustrates the subtle variations in horizontal and moment bearing capacities across these scour angles.

Analysis reveals that, consistent with Guo et al. (2022), an increase in scour angle leads to a slight but noticeable improvement in bearing capacity. However, as the scour angle continues to rise, the rate of capacity growth gradually slows. This suggests that both horizontal and moment bearing capacities may eventually stabilize at a constant value with further increases in scour angle.

These insights enhance our understanding of the effects of scour angle and reinforce earlier findings on the influence of scour depth and width on caisson bearing capacity. This holistic view highlights the complex interplay of various parameters, providing valuable guidance for the robust design of caisson foundations in sandy soil under different scour conditions.

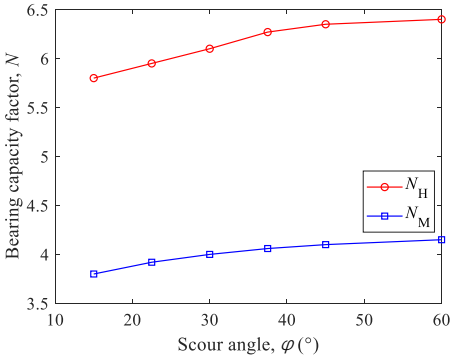

Figure 9 Bearing capacity factors with different scour angles

4 EFFECT OF LOCAL SCOUR ON THE EVOLUTION OF FAILURE ENVELOPE

Section 3 examined the effects of scour depth, width, and angle on the bearing capacities of the suction caisson under horizontal and moment loading conditions. It was found that scour depth has the most significant impact on bearing capacity, compared to scour width and angle. Therefore, this section focuses on the variation of bearing capacity envelopes at different scour depths, while keeping the scour width (S_w/D=0.5) and scour angle (φ=30°) constant. As noted earlier, the suction caisson foundation is more influenced by horizontal and moment loadings during normal service conditions, so this section primarily investigates the bearing capacity envelopes in the *H-M* plane.

According to Gottardi et al. (1999), two loading control methods are typically used to establish the failure envelope of a foundation: (1) **Swipe tests** and (2) **Radial displacement tests**. In this analysis, radial displacement tests are adopted as the primary method for controlling loading. To examine the failure surface in the *H-M* plane, various loading paths are applied to the Loading Reference Point (LRP) of the caisson, as shown in Figure 10. Sufficiently large displacement values are selected to ensure the maximum strength is reached.

Figure 11 shows examples of load paths for a relative scour depth S_d/L=0.3 in the *H-M* plane, obtained from various radial displacement tests. A constant ratio between the increments of rotation (θ) and horizontal displacement (u) (i.e., $\delta\theta/\delta u$ constant) indicates a straight loading path, as shown in Figure 11(a). By connecting the endpoint values of the different load paths, the failure envelope is derived, as illustrated in Figure 11(b).

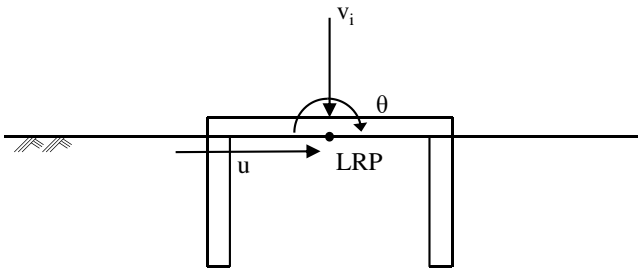

Figure 10 Schematic plot of radial displacement tests

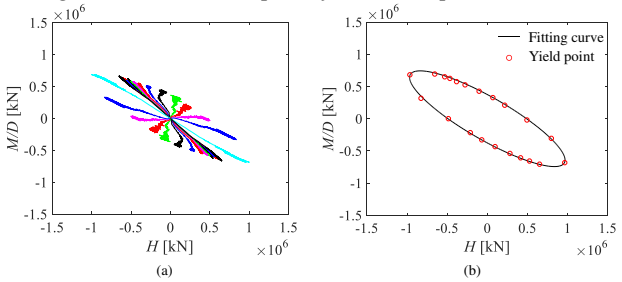

Figure 11 Radial displacement control tests in the H-M plane: (a) load paths, and (b) failure surface

It is essential to note that for the radial loading paths to accurately approximate the extreme capacity diagram, the displacement must be sufficiently large to ensure the maximum strength is reached. As shown in Figure 11, most loading paths lead to the ultimate bearing capacity, marked by distinct inflection points. However, for some paths, achieving the ultimate bearing capacity remains challenging, even with

substantial displacements. To provide a consistent basis for determination, the ultimate load capacity is defined by the endpoint values of the load paths, which are then used to establish the final failure envelope.

To quantify the impact of scour depth on failure envelope, a modified analytical equation is proposed here based on the original formula reported by Villalobos et al. (2009):

$$y=\left(\frac{H}{h_i H_0}\right)^2+\left(\frac{M}{Dm_i H_0}\right)^2+2e\frac{H}{h_i H_0}\frac{M}{Dm_i H_0}-1=0 \quad (1)$$

The general form of failure surface is described by h_i, m_i, and e. The fitting parameters h_i and m_i indicate the intersections of each ellipse with the H/H_0 and M/DH_0 axes (where H_0 represents the horizontal bearing capacity without considering local scour), respectively. Meanwhile, e represents the eccentricity of each ellipse. By utilizing Eq.(1), the yield points obtained from simulated results can be accommodated through a least-squares regression.

Eq.(1) represents the typical implicit ellipse equation. The more common expression for the ellipse equation is:

$$AX^2+BXY+CY^2+DX+EY+F=0 \quad (2)$$

By simultaneously considering Eq. (1) and (2), The expressions for h_i, m_i, and e can be obtained as follows:

$$\begin{cases} h_i=\dfrac{ab}{H_0\sqrt{a^2\sin^2\phi+b^2\cos^2\phi}} \\ m_i=\dfrac{ab}{DH_0\sqrt{a^2\cos^2\phi+b^2\sin^2\phi}} \\ e=\dfrac{\sin\phi\cos\phi\left(a^2-b^2\right)}{\sqrt{\left(a^2\sin^2\phi+b^2\cos^2\phi\right)\left(a^2\cos^2\phi+b^2\sin^2\phi\right)}} \end{cases} \quad (3)$$

It is noticeable that, as scour depth changes, the inclination angle of the failure envelope remains unchanged. This means that the eccentricity of the ellipse remains constant. Hence, to quantify the influence of scour depth variations on the failure envelope, it is sufficient to establish the relationship between relative scour depth and the parameters h_i, m_i. Computational analysis reveals that the parameters h_i and m_i exhibit the following relationship with depth variations:

$$\begin{cases} h_i=\left(1-0.82\dfrac{S_d}{L}\right)h_0 \\ m_i=\left(1-0.77\dfrac{S_d}{L}\right)m_0 \end{cases} \quad (4)$$

In Eq. (4), h_0 and m_0 denote the parameters of the fitted ellipse for the failure envelope without local scour, i.e. S_d/L=0. Figure 12 compares the results of Eq. (1) to the simulation results for the failure envelope in the *H-M* plane. Good agreements could be observed while considering various scour depths. This confirms that Eq. (6) effectively captures the degree of impact of scour depth on the failure envelope.

Based on the previous discussions, the proposed design procedure for the caisson, incorporating the effects of local scour, is as follows:

(step i) Obtain three characteristic parameters: the semi-major axis length a, the semi-minor axis length b, and the rotation angle Φ. These can be measured directly or calculated using empirical formulas from previous studies (Jin Z. et al., 2019).

(step ii) Calculate the shape fitting parameters h_0, m_0, and e using Equation 3, without considering local scour. The horizontal bearing capacity H_0 can be determined through numerical simulations.

(step iii) For a specific relative scour depth S_d/L, determine the shape fitting parameters h_i and m_i using Equation 4.

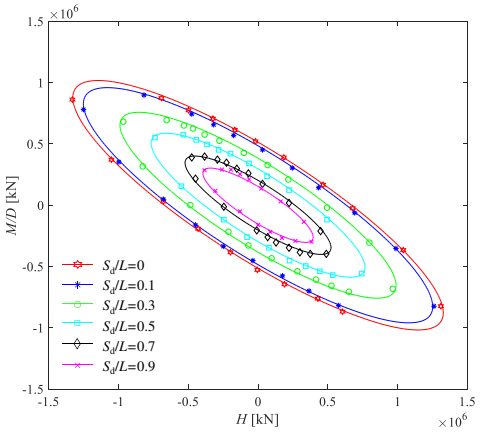

Figure 12 Fitting curves by the analytical equation and numerical results for various scour depths

5 CONCLUSIONS

This study used finite element simulations to examine the response of caisson foundations under various scour conditions, including scour depth, width, and angle. An empirical formula was developed to characterize the failure envelope in the *H-M* plane, accounting for scour depth.

Key findings include:

1. Horizontal bearing capacity is more sensitive to scour depth, showing a larger reduction. Both horizontal and moment bearing capacities stabilize when the relative scour depth exceeds 0.9, with no further capacity reduction.

2. The impact of scour width and angle is less significant than that of scour depth. Therefore, the study mainly focuses on scour depth, using typical scour width and angle values.
3. Scour depth alters the size of the failure envelope, but its shape remains elliptical. This makes it easy to integrate normalized scour depth into existing failure envelope equations.

These findings provide valuable insights for assessing the safety of offshore structures in scour-prone environments and can inform the development of simplified modeling approaches, such as the macroelement method.

AUTHOR CONTRIBUTION STATEMENT

Zhuang JIN: Data curation, Formal Analysis, Writing- Original draft. **Yin-Fu JIN**: Software, Conceptualization, Methodology, Supervision. **Meng-Huan GUO:** Resources, Conceptualization, Writing – review & editing, Supervision, Project administration, Funding acquisition.

ACKNOWLEDGEMENTS

This research was financially supported by the National Natural Science Foundation of China (Grant No.: 52308364, 52278363, 52090084, 51938008), Shenzhen Science and Technology Program (Grant No. KQTD20221101093555006), the Research Grants Council (RGC) of Hong Kong Special Administrative Region Government (HKSARG) of China (Grant No.: 15217220, 15229223, N_PolyU534/20) and the Hong Kong Polytechnic University Strategic Importance Fund (ZE2T) and Project of Research Institute of Land and Space (CD78).

REFERENCES

AASHTO, B.D.S., 2010. American Association of State Highway and Transportation Officials. Washington, DC 4.

ABAQUS, I., 2014. Abaqus documentation. Version 6, 5-1.

Arneson, L., 2013. Evaluating scour at bridges. United States. Federal Highway Administration.

Chen, X., Xu, J., Qin, H., Zhou, L., Ma, T., Liu, X., Liu, J., 2019. Model test study on horizontal static loading of suction bucket foundation under different scour conditions. Journal of Testing and Evaluation 47 (4), 3185-3208.

Gottardi, G., Houlsby, G., Butterfield, R., 1999. Plastic response of circular footings on sand under general planar loading. Géotechnique 49 (4), 453-470.

Guo, X., Liu, J., Yi, P., Feng, X., Han, C., 2022. Effects of local scour on failure envelopes of offshore monopiles and caissons. Applied Ocean Research 118, 103007.

Houlsby, G., Byrne, B., 2004. Calculation procedures for installation of suction caissons. Report No. OUEL2268/04, University of Oxford.

Houlsby, G.T., Kelly, R.B., Huxtable, J., Byrne, B.W., 2005. Field trials of suction caissons in clay for offshore wind turbine foundations. Géotechnique 55, 287-296.

Ibsen, L.B., Liingaard, S., Nielsen, S.A., 2005. Bucket Foundation, a status. Proceedings of the Copenhagen Offshore Wind.

Jin, Y.-F., Yin, Z.-Y., Shen, S.-L., Zhang, D.-M., 2017. A new hybrid real-coded genetic algorithm and its application to parameters identification of soils. Inverse Problems in Science and Engineering 25 (9), 1343-1366.

Jin Z., Yin Z-Y, Kotronis P., Z., L., 2019. Advanced numerical modelling of caisson foundations in sand to investigate the failure envelope in the H-M-V space. Ocean Engineering 190, 106394.

Liang, F., Wang, C., Huang, M., Wang, Y., 2017. Experimental observations and evaluations of formulae for local scour at pile groups in steady currents. Marine Georesources & Geotechnology 35 (2), 245-255.

Lin, C., Han, J., Bennett, C., Parsons, R.L., 2014. Analysis of laterally loaded piles in sand considering scour hole dimensions. Journal of geotechnical and geoenvironmental engineering 140 (6), 04014024.

Lin, Y., Lin, C., 2019. Effects of scour-hole dimensions on lateral behavior of piles in sands. Computers and Geotechnics 111, 30-41.

Lin, Y., Lin, C., 2020. Scour effects on lateral behavior of pile groups in sands. Ocean Engineering 208, 107420.

Liu, J., Chen, X., Zhu, Z., Wang, B., 2019. Investigation of scour effect on tensile capacity of suction caissons considering stress history of sand. Marine Georesources & Geotechnology 37 (9), 1044-1056.

Villalobos, F.A., Byrne, B.W., Houlsby, G.T., 2009. An experimental study of the drained capacity of suction caisson foundations under monotonic loading for offshore applications. Soils and foundations 49 (3), 477-488.